ratios recorded by the mass spectrometers during AUV and rosette operations are in close agreement with Winkler data (Fig. 4A), exhibiting no statistically significant correlation between oxygen and hydrocarbon levels (Fig. 4B). Given that the manufacturer of the oxygen microelectrode sensor advises that hydrocarbon contamination can affect its performance (*24*), we propose that hydrocarbon contamination could explain some of the low oxygen excursions we observed using this sensor.

The lack of systematic oxygen drawdown within the plume suggests that the petroleum hydrocarbons did not fuel appreciable microbial respiration on the temporal scales of our study. Assuming that the aforementioned west-southwest current carried the hydrocarbon-rich layer away from the well site at the measured velocity of ~7.8 cm s^{-1} (~6.7 km d^{-1}), the plume at the end of our survey 35 km from the well site was at least 5 days old. Based on the 95% confidence interval of our Winkler oxygen data from the plume layer (±2 μM), we estimate that microbial respiration in the plume was not appreciably more than ~0.8 μM O_2 per day or, based on elemental formula for straight-chain hydrocarbons, ~0.5 μM C per day. This suggests that if the hydrocarbons are indeed susceptible to biodegradation, then it may require many months before microbes substantially attenuate the hydrocarbon plume to the point that oxygen-minimum zones develop that are intense enough {[O_2] < 63 μM (*25*, *26*)} to threaten Gulf of Mexico fisheries.

References and Notes

1. Unified Command Deepwater Horizon, "U.S. Scientific Teams Refine Estimates of Oil Flow from BP's Well Prior to Capping," Gulf of Mexico Oil Spill Response 2010 [cited 2 August 2010]; available at www.deepwaterhorizonresponse.com/go/doc/2931/840475/.
2. Ø. Johansen, *Mar. Pollut. Bull.* **47**, 360 (2003).
3. Ø. Johansen, *Spill Sci. Technol. Bull.* **6**, 103 (2000).
4. D. Simecek-Beatty, W. J. Lehr, in *Oil Spill Environmental Forensics*, Z. Wang, S. A. Stout, Eds. (Academic Press, Burlington, MA, 2007), chap. 13, pp. 405–418.
5. F. Chen, P. D. Yapa, *J. Mar. Syst.* **45**, 189 (2004).
6. L. K. Dasanayaka, P. D. Yapa, *J. Hydro-Environ. Res.* **2**, 243 (2009).
7. Supporting material is available on *Science* Online.
8. R. Camilli, A. N. Duryea, *Environ. Sci. Technol.* **43**, 5014 (2009).
9. C. R. German *et al.*, *Deep-Sea Res. Part I Oceanogr. Res. Pap.* **55**, 203 (2008).
10. D. L. Valentine *et al.*, *Nat. Geosci.* **3**, 345 (2010).
11. S. Mau *et al.*, *Geophys. Res. Lett.* **34**, L22603 (2007).
12. R. Camilli, A. Duryea, in *Proc. IEEE/MTS OCEANS 2007* (IEEE/MTS, Vancouver, Canada, 2007), pp. 1–7 (10.1109/OCEANS.2007.4449412).
13. R. Camilli, B. Bingham, C. M. Reddy, R. K. Nelson, A. N. Duryea, *Mar. Pollut. Bull.* **58**, 1505 (2009).
14. C. R. German, K. J. Richards, M. D. Rudnicki, M. M. Lam, J. L. Charlou, *Earth Planet. Sci. Lett.* **156**, 267 (1998).
15. Monterey Bay Aquarium Research Institute, "Data Report NOAA Ship *Gordon Gunter* Cruise GU-10-02, Gulf of Mexico June 2–3, 2010 Operations of the MBARI AUV *Dorado*" [cited 28 July 2010]; available at www.noaa.gov/sciencemissions/PDFs/MBARI_AUV_DataReport_GU-10-02.pdf.
16. Z. Wang, M. Fingas, M. Landriault, L. Sigouin, N. Xu, *Anal. Chem.* **67**, 3491 (1995).
17. K. A. Kvenvolden, C. K. Cooper, *Geo-Mar. Lett.* **23**, 140 (2003).
18. J. Gillis, "Giant plumes of oil forming under the Gulf," *New York Times*, 16 May 2010, p. A1.
19. S. Goldenberg, "Biologists find 'dead zones' around BP oil spill in Gulf," *The Guardian*, 1 July 2010, p. 26.
20. Inter-Agency Joint Analysis Group, "Review of Preliminary Data to Examine Subsurface Oil In the Vicinity of MC252#1 May 19 to June 19, 2010" [cited 23 July 2010]; available at http://ecowatch.ncddc.noaa.gov/JAG/files/JAG%20Data%20Report%202%20FINAL.pdf.
21. L. W. Winkler, *Ber. Dtsch. Chem. Ges.* **21**, 2843 (1888).
22. C. Oudot, R. Gerard, P. Morin, I. Gningue, *Limnol. Oceanogr.* **33**, 146 (1988).
23. H. E. Garcia, R. A. Locarnini, T. P. Boyer, J. I. Antonov, in *World Ocean Atlas 2005*, *vol. 3: Dissolved Oxygen, Apparent Oxygen Utilization, and Oxygen Saturation*, S. Levitus, Ed. (U.S. Government Printing Office, Washington, DC, 2006), p. 342.
24. Sea-Bird Electronics, "SBE 43 Dissolved Oxygen Sensor – Background Information, Deployment Recommendations, and Cleaning and Storage," Application Note No. 64 (February 2010); available at www.seabird.com/application_notes/AN64.htm.
25. L. H. Stevenson, B. Wyman, in *Dictionary of Environmental Science* (Facts on File, New York, 1991), p. 294.
26. N. N. Rabalais *et al.*, *Biogeosciences* **7**, 585 (2010).

27. This research was supported by NSF grants OCE-1045025 (RAPID Response Research) and OCE-0537173 (National Oceanographic Partnership Program for *TETHYS* development) to R.C., OCE-1043976 (RAPID) to C.M.R., OCE-1045670 (RAPID) to B.A.S.V.M., and OCE-0644290 [NSF Ocean Sciences (OCE)–Submersible] for *Sentry* development and integration to D.R.Y.; by U.S. Coast Guard HSCG3210CR0020 to R.C.; and by NASA Astrobiology Science and Technology for Exploring Planets (ASTEP) NNX09AB76G for integrating technology with *Sentry* to D.R.Y. We thank the officers and crew of the R/V *Endeavor* and J. Parker and J. Kusek of the U.S. Coast Guard for assistance during marine operations at the Deepwater Horizon well site. We thank K. Keteles (U. S. Environmental Protection Agency); D. Hollander and E. Goddard (Univ. of South Florida); and A. Billings, A. Duester, S. McCue, D. Torres, M. Swartz, C. Murphy, R. Catanach, and J. Fenwick (Woods Hole Oceanographic Institution) for logistics, operations, experimental, and administrative support. We acknowledge J. Ledwell, C. German, R. Munier, and especially J. Farrington for valuable discussions and guidance.

Supporting Online Material

www.sciencemag.org/cgi/content/full/science.1195223/DC1
SOM Text
Figs. S1 to S12
Tables S1 and S2
References

16 July 2010; accepted 13 August 2010
Published online 19 August 2010;
10.1126/science.1195223
Include this information when citing this paper.

Deep-Sea Oil Plume Enriches Indigenous Oil-Degrading Bacteria

Terry C. Hazen,[1]* Eric A. Dubinsky,[1] Todd Z. DeSantis,[1] Gary L. Andersen,[1] Yvette M. Piceno,[1] Navjeet Singh,[1] Janet K. Jansson,[1] Alexander Probst,[1] Sharon E. Borglin,[1] Julian L. Fortney,[1] William T. Stringfellow,[1,2] Markus Bill,[1] Mark E. Conrad,[1] Lauren M. Tom,[1] Krystle L. Chavarria,[1] Thana R. Alusi,[1] Regina Lamendella,[1] Dominique C. Joyner,[1] Chelsea Spier,[2] Jacob Baelum,[1] Manfred Auer,[1] Marcin L. Zemla,[1] Romy Chakraborty,[1] Eric L. Sonnenthal,[1] Patrik D'haeseleer,[4] Hoi-Ying N. Holman,[1] Shariff Osman,[1] Zhenmei Lu,[3] Joy D. Van Nostrand,[3] Ye Deng,[3] Jizhong Zhou,[1,3] Olivia U. Mason[1]

The biological effects and expected fate of the vast amount of oil in the Gulf of Mexico from the Deepwater Horizon blowout are unknown owing to the depth and magnitude of this event. Here, we report that the dispersed hydrocarbon plume stimulated deep-sea indigenous γ-Proteobacteria that are closely related to known petroleum degraders. Hydrocarbon-degrading genes coincided with the concentration of various oil contaminants. Changes in hydrocarbon composition with distance from the source and incubation experiments with environmental isolates demonstrated faster-than-expected hydrocarbon biodegradation rates at 5°C. Based on these results, the potential exists for intrinsic bioremediation of the oil plume in the deep-water column without substantial oxygen drawdown.

Assessing the environmental and public health impacts of the Deepwater Horizon blowout is difficult owing to the extreme depth of the blowout and the large volumes of oil released. Moreover, the effectiveness of the primary initial mitigation strategy (e.g., injecting the oil dispersant Corexit 9500 directly at the wellhead in a water depth of 1544 m) is difficult to assess despite initial analysis of its potential toxicity (*1*). An optional strategy for remediation of the deep underwater plume is to use the intrinsic bioremediation potential of deep-sea microorganisms to degrade the oil. This strategy depends on a number of environmental factors, including a favorable response of indigenous microorganisms to an increased concentration of hydrocarbons and/or dispersant.

To determine the impact of the deep hydrocarbon plume on the marine microbes residing in the plume and the rates of hydrocarbon biodegradation, we collected deep-water samples from two ships between 25 May 2010 and 2 June 2010. In total, we analyzed the physical, chemical, and microbiological properties (fig. S1) of 17 deep-water samples from across the Gulf of Mexico (*2*).

[1]MS 70A-3317, One Cyclotron Road, Lawrence Berkeley National Laboratory, Berkeley, CA 94720, USA. [2]University of the Pacific, Ecological Engineering Research Program, 3601 Pacific Avenue, Stockton, CA 95211, USA. [3]University of Oklahoma, 101 David L. Boren Boulevard, Norman, OK 73072, USA. [4]Biosciences and Biotechnology Division, Lawrence Livermore National Laboratory, Livermore, CA 94550, USA.

*To whom correspondence should be addressed. E-mail: tchazen@lbl.gov

We detected a deep-sea oil plume from 1099 to 1219 m at distances of up to 10 km from the wellhead (fig. S2). Owing to its composition (fig. S3), the plume was likely dispersed MC252 oil, a conclusion also reached by Camilli *et al.* (*3*). At most locations where the plume was detected, there was a slight decrease in oxygen concentration indicative of microbial respiration and oxygen consumption, as would be expected if the hydrocarbons were being catabolized (Fig. 1). Oxygen saturation within the plume averaged 59%, while outside the plume it was 67%. Extractable hydrocarbons (e.g., octadecane) ranged from nondetectable in the nonplume samples to 9.21 μg/liter in plume samples (table S1). Volatile aromatic hydrocarbons were significantly higher in the plume interval (mean 139 μg/liter) than in the nonplume samples from similar depths. The average temperature within the plume interval was 4.7°C and the pressure was 1136 dB. Soluble orthophosphate, and total ammonia-N, were detected at similar concentrations within and outside the plume interval (table S1).

The dispersed oil plume affected both microbial cell densities and composition (Fig. 1 and table S1). Cell densities in the plume ($5.51 \pm 0.33 \times 10^4$ cells/ml) were higher than outside the plume ($2.73 \pm 0.05 \times 10^4$ cells/ml). Phospholipid fatty acid analysis also confirmed an increase in microbial biomass in the plume (0.57 pmol lipids/ml) versus outside the plume (0.23 pmol lipids/ml) (table S1). In addition to the observed increase in cell densities, PhyloChip 16*S* ribosomal RNA (rRNA) microarray analysis (fig. S4) suggests that the plume significantly altered the microbial community composition and structure. Ordination of bacterial and archaeal 16*S* rRNA gene composition revealed two distinct clusters of samples: one composed entirely of plume samples with detected oil and the other of nonplume samples (Fig. 2). No physical or chemical factors other than hydrocarbons and nitrates were significantly different between these groups (table S1), indicating that microorganisms were responding directly to the presence of dispersed oil.

In plume samples, PhyloChip analysis revealed that 951 distinct bacterial taxa in 62 phyla were present (fig. S4), but only 16 distinct taxa that were all classified as γ-Proteobacteria were significantly enriched in the plume relative to nonplume samples (table S2 and fig. S5). Nearly all

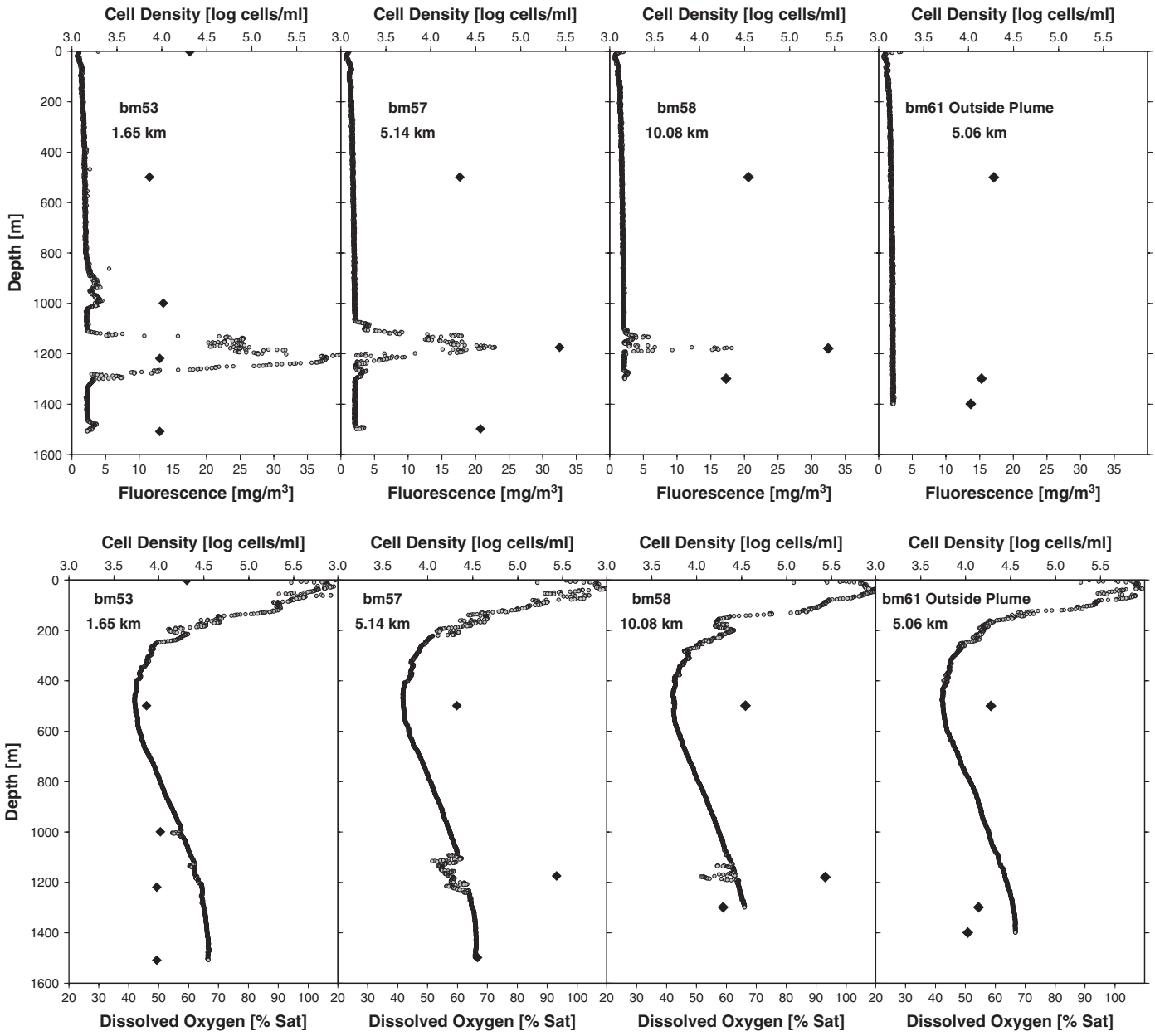

Fig. 1. Characteristic depth profiles of cell density, fluorescence, and dissolved oxygen for distances from the source (BM53, BM57, and BM58) and one nonplume site (BM61). Diamonds indicate cell density.

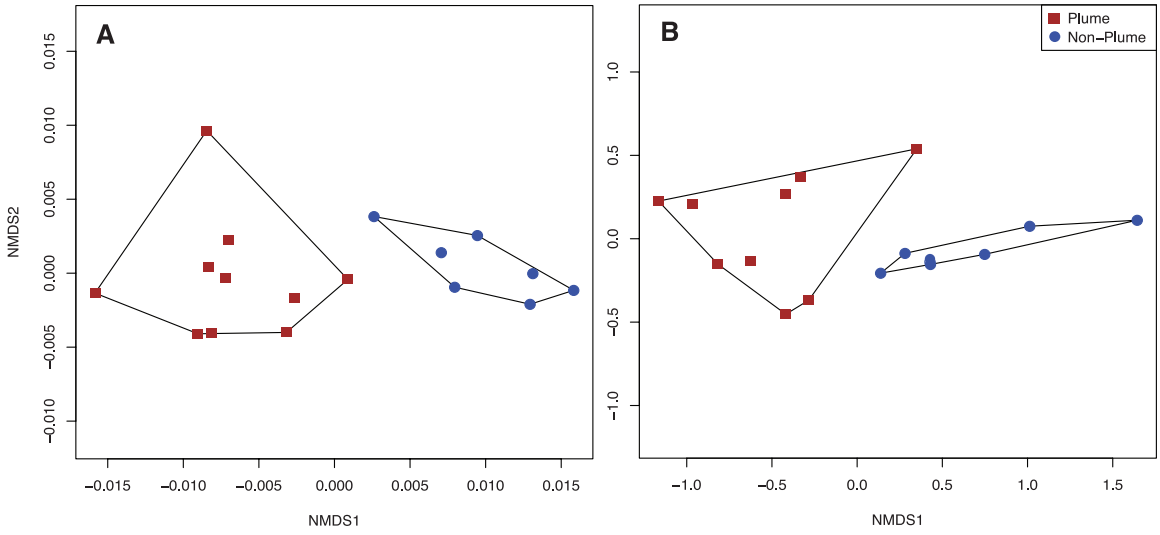

Fig. 2. Microbial community analysis of deep-water plume and nonplume samples. Differences in composition of (**A**) 16*S* rRNA gene sequences measured by PhyloChip and (**B**) phospholipid fatty acids were analyzed with nonmetric multidimensional scaling ordination of Bray-Curtis distances (stress = 3.98 and 4.55, respectively). Plume and nonplume communities were significantly different as determined by permutational analysis of variance ($P = 0.005$ for both) and delineated with lines for clarity.

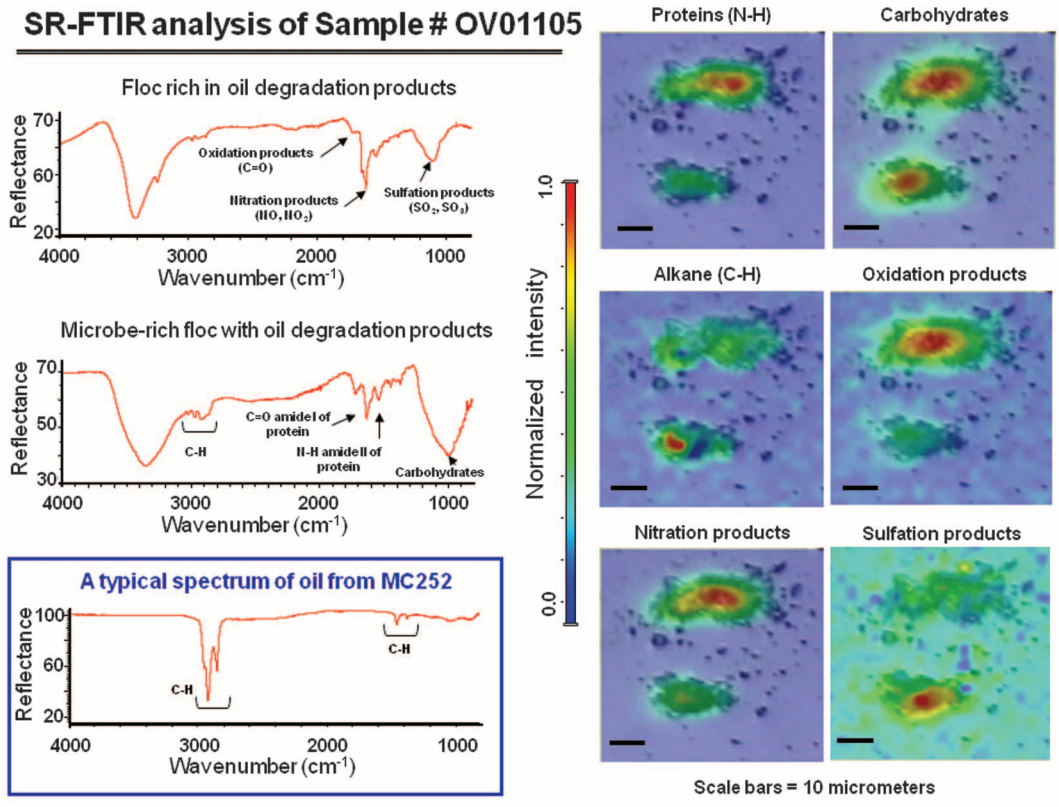

Fig. 3. SR-FTIR images (~60 μm by 60 μm) showing the distribution of microorganisms, oil, and oil degradation products in a "floc." Distribution heat map of the protein amide II vibration modes at ~1542 cm^{-1} and the carbohydrates vibration modes at ~1000 cm^{-1} (*20*). Distribution heat map of alkane C-H vibration modes in oil from MC252. Distribution heat map of carbonyl (C=O) vibration modes at ~1730 cm^{-1} in oil oxidation products, of nitrogen oxides vibration modes at ~1610 cm^{-1} in nitration products, and of sulfur oxides vibration modes at ~1150 cm^{-1} in sulfation products. Scale bars: 10 μm. Reflectance is given in percentage units.

of these enriched taxa have representatives that degrade hydrocarbons or are stimulated by the presence of oil in cold environments (table S2). Plume-enriched bacteria include many psychrophilic and psychrotolerant species that have been observed in low-temperature marine environments (table S2) (*4*–*6*). Although cell densities are higher in the plume, taxonomic richness was lower and the diversity of enriched bacteria was restricted to a few γ-Proteobacteria.

Cloning and sequencing revealed that deep-sea plume samples from station BM58 (~10.08 km from the MC252 wellhead) and station OV011 (~1.5 km from the wellhead) were dominated by the order *Oceanospirillales* in the γ-Proteobacteria. More than 90% of all sequences in both plume samples (10 km between sampling stations) belonged to a single operational taxonomic unit (OTU) that is most closely related to *Oceanospirillales* (Fig. 3). In a control sample (site OV003) collected 39.1 km southwest of the wellhead, this same OTU represented only 5% of all sequences analyzed (Fig. 3). In addition, this taxon was detected in all 10 oil plume samples analyzed by the PhyloChip and was significantly enriched relative to background deep seawater with no oil (table S1). The cultured representatives most closely related to the OTU in plume samples were *Spongiispira norvegica* (95% similar) and *Oceaniserpentilla haliotidis* (94% similar). The observed sequences in the plume samples form a clade with two distinct *Oceanospirillales* groups. One of these groups is largely composed of known psychrophilic hydrocarbon degraders and microorganisms from hydrocarbon-dominated environments (*5*, *7*, *8*), including *Oleispira antarctica*, *Thalassolituus oleivorans*, and *Oleiphilus messinensis* (fig. S5).

The three dominant phospholipid fatty acids detected in the plume samples were C16:0,

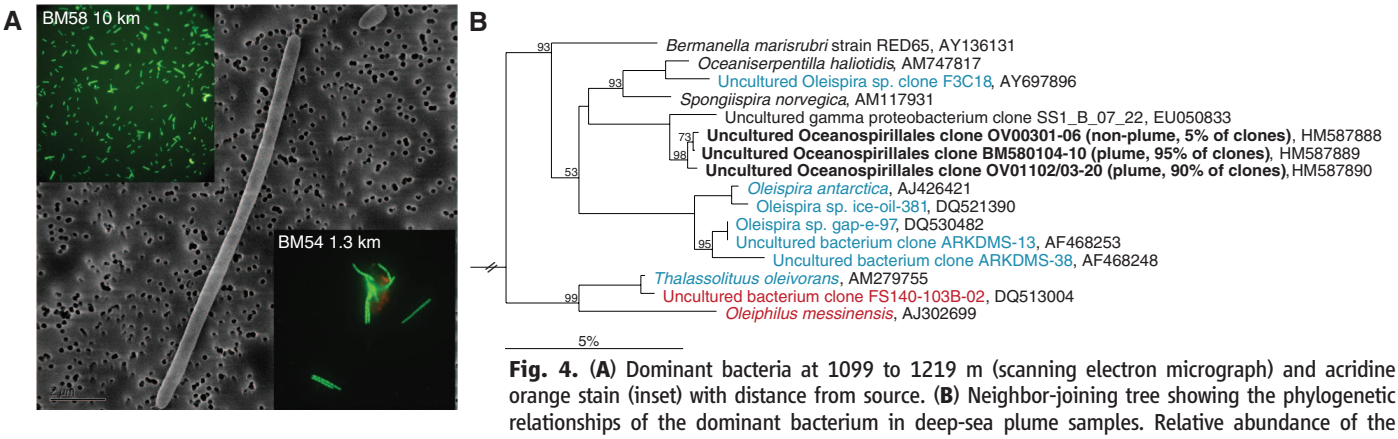

Fig. 4. (**A**) Dominant bacteria at 1099 to 1219 m (scanning electron micrograph) and acridine orange stain (inset) with distance from source. (**B**) Neighbor-joining tree showing the phylogenetic relationships of the dominant bacterium in deep-sea plume samples. Relative abundance of the dominant bacterium was 90 to 95% of plume samples and 5% of the nonplume sample (shown in parentheses). Psychrophilic, hydrocarbon-degrading bacteria, as well as uncultured organisms from low-temperature, hydrocarbon-dominated environments, are shown in blue. Organisms shown in red are either known hydrocarbon degraders or are from hydrocarbon-dominated ecosystems but are not from low-temperature environments. Bootstrap values based on 1000 replicates of ≥50% are shown at branch points. *Aquifex pyrophilus* (GenBank accession M83548) was used as the outgroup.

C16:1w7c, and C18:1w9c (table S3), which have been reported as the dominant lipids in the *Oleispirea antarctica*, in some strains of the *Oceaniserpentilla haliotis* (*4*), and in a consortium of marine hydrocarbon-degrading bacteria (*9*). 18:1w9t/c ratios that have been reported to increase in oil-contaminated environments (*10*, *11*) were slightly elevated in plume samples (average 0.21) compared to nonplume samples (average 0.14) but were not strongly correlated with oil concentrations (table S1). Multivariate analysis of phospholipid fatty acid (PLFA) profiles from each sample revealed distinct clustering of plume and nonplume samples similar to community analysis of microarray data (Fig. 2).

Microscopic examination of cells collected within the plume also revealed that the dominant cell type exhibits a distinctive morphology typical of the *Oceanospirillales* (Fig. 4). Total bacterial densities were also significantly correlated with MC252 alkane concentration in the plume (fig. S5). Synchrotron radiation–based Fourier-transform infrared (SR-FTIR) spectromicroscopy revealed absorptions at ~1730, ~1610, and ~1150 cm^{-1} that are associated with biomolecule-rich regions of a cellular floc (Fig. 3). These absorption features are well described for the carbonyl (C=O), nitrogen oxides, and sulfur oxides vibration modes (*12*) and are characteristic of oil degradation products (*13*). These SR-FTIR spectra are not consistent with those typically found in marine macroaggregates (*14*), nor are they consistent with nonplume samples at the same depth.

To understand the distribution of oil-degrading genes within the plume, we analyzed five samples (BM053, BM054, BM057, BM058, BM064) from the MC252 dispersed oil plume as well as five uncontaminated, control samples (OV003, OV004, OV009, OV013 and OV014) collected from plume depth with GeoChip functional array (table S4) (*15*, *16*). Altogether, 4000 to 5000 functional genes were detected per sample, among which 1652 genes are involved in hydrocarbon degradation. Detrended correspondence analysis showed that microbial community functional composition and structure were considerably different between oil-plume and nonplume control samples (fig. S7), which is consistent with PhyloChip analysis. Many of the genes involved in hydrocarbon degradation were significantly ($P < 0.05$ or 0.01) increased in oil plume samples (figs. S8 and S9). Statistical analysis by Mantel test showed that the overall microbial functional composition and structure were significantly correlated with many key oil contaminants, including isopropylbenzene, *n*-propylbenzene, *tert*-butylbenzene, 1,2,4-trimethylbenzene, *p*-isopropyltoluene, *n*-butylbenzene, and naphthalene (table S5). Analysis based on individual genes showed that the changes of many hydrocarbon degradation genes are significantly correlated with the concentrations of oil contaminants (table S6). For instance, the *phdCI* gene encoding carboxylate isomerase for naphthalene degradation correlates with several hydrocarbons (table S6). These results indicated that a variety of hydrocarbon-degrading populations exist in the deep-sea plume and that the microbial communities appear to be undergoing rapid dynamic adaptation in response to oil contamination. These results also imply that there exists a potential for intrinsic bioremediation of oil contaminants in the deep sea and that oil-degrading communities could play an important role in controlling the ultimate fates of hydrocarbons in the Gulf.

The bioremediation potential largely depends on the rates of biodegradation in the plume. We calculated maximum biodegradation rates using two data sets from the field and two from laboratory microcosms representing concentrations of C13 to C26 *n*-alkanes (table S7). The degradation rate coefficients and half-life values (table S7 and figs. S10 and S11), calculated from the alkane data from these four sources with the first-order rate equation (*10*, *17*), are similar to those reported for comparable temperature and field conditions (*10*, *17*–*19*). Despite the varying field and microcosm conditions, the oil half-lives are 1.2 to 6.1 days (table S7). The field half-lives should in part reflect the effect of mixing and dilution, but the similarity of the rate of disappearance of alkanes in the plume to the rates observed in the laboratory suggest it is possible that the actual degradation of alkanes lies within this range. The possibility that biodegradation largely controls the disappearance of alkanes is also supported by the preferential degradation of short-chain alkanes, as represented in the increase in the ratio of C26/C15 alkanes over 10 km, from less than 1 to more than 3 (fig. S18). For each data set, decay constants were similar for all alkanes measured in all samples, with the exception of the plume samples from the nonlipid fraction collected on 0.2-μm filters. Because these results represent extraction from free-phase oil or oil absorbed to the membrane filter, it is likely that the higher rates seen for the shorter-chain alkanes are due to additional losses in collected sample resulting from dissolution into seawater; however, there is a correlation of longer-chain alkane concentration with cell densities in the plume (fig. S6). The oil biodegradation rates reported here at 5°C are explained partly by the relatively light nature of this crude (which contains a large volatile component that is more readily degraded), the dispersed nature of the deep plume (small oil particle size), the low overall concentrations of oil in the deep plume, and the frequent episodic oil leaks from natural seeps in this area that the deep-sea microbial community may have adapted to over long periods of time.

References and Notes

1. R. S. Judson *et al.*, *Environ. Sci. Technol.* **44**, 5979 (2010).
2. Materials and methods are available on *Science* Online.
3. R. Camilli *et al.*, *Science* **330**, 201 (2010); published online 19 August 2010 (10.1126/science.1195223).
4. A. Schlösser, A. Lipski, J. Schmalfuss, F. Kugler, G. Beckmann, *Int. J. Syst. Evol. Microbiol.* **58**, 2122 (2008).
5. M. M. Yakimov *et al.*, *Int. J. Syst. Evol. Microbiol.* **53**, 779 (2003).
6. M. M. Yakimov, K. N. Timmis, P. N. Golyshin, *Curr. Opin. Biotechnol.* **18**, 257 (2007).
7. G. Gentile *et al.*, *Environ. Microbiol.* **8**, 2150 (2006).
8. M. M. Yakimov *et al.*, *FEMS Microbiol. Ecol.* **49**, 419 (2004).
9. E. Aries, P. Doumenq, J. Artaud, M. Acquaviva, J. C. Bertrand, *Org. Geochem.* **32**, 891 (2001).

10. S. J. MacNaughton *et al.*, *Appl. Environ. Microbiol.* **65**, 3566 (1999).
11. S. M. Pfiffner *et al.*, *Geomicrobiol. J.* **23**, 431 (2006).
12. G. Socrates, *Infrared and Raman Characteristics Group Frequencies—Tables and Charts* (Wiley, Chichester, UK, ed. 3, 2001).
13. N. Robinson, *Wearcheck Tech. Bull.* (2000); www.machinerylubrication.com/Read/1109/oil-degradation-spectroscopy.
14. N. Kovac, O. Bajt, J. Faganeli, B. Sket, B. Orel, *Mar. Chem.* **78**, 205 (2002).
15. Z. He *et al.*, *ISME J.* **4**, 1167 (2010).
16. Z. L. He *et al.*, *ISME J.* **1**, 67 (2007).
17. A. D. Venosa, E. L. Holder, *Mar. Pollut. Bull.* **54**, 545 (2007).
18. R. Atlas, J. Bragg, *Microb. Biotechnol.* **2**, 213 (2009).
19. O. G. Brakstad, K. Bonaunet, *Biodegradation* **17**, 71 (2006).
20. D. Naumann, in *Encyclopedia of Analytical Chemistry*, R. Meyers, Ed. (Wiley, Chichester, UK, 2000), pp. 102–131.
21. This work was supported by a subcontract from the University of California at Berkeley, Energy Biosciences Institute, to Lawrence Berkeley National Laboratory under U.S. Department of Energy contract DE-AC02-05CH11231 and by the University of Oklahoma Research Foundation. The Energy Biosciences Institute is funded by British Petroleum. The SR-FTIR work was conducted at the infrared beamline at the Advanced Light Source, which is supported by the Director, Office of Science, Office of Basic Energy Sciences, of the U.S. Department of Energy. We thank T. Pollard, K. Keller, M. Carrera, P. Willems, P. Carragher, P. Collinson, S. Lisiecki, P. Vaishampayan, R. Graham, J. Wong, N. Duncan, D. Long, and N. Tam for logistical and technical support. We also thank the captain, crew, and science teams aboard the R/V *Ocean Veritas* and the R/V *Brooks McCall*. The National Center for Biotechnology Information accession numbers of the 16*S* rRNA genes retrieved from clone library analyses are HM587888, HM587889, and HM587890. Sequences for 16*S* rRNA are also available at greengenes.lbl.gov.

Supporting Online Material

www.sciencemag.org/cgi/content/full/science.1195979/DC1
Methods
Figs. S1 to S18
Tables S1 to S8
References

2 August 2010; accepted 20 August 2010
Published online 24 August 2010;
10.1126/science.1195979
Include this information when citing this paper.

Propane Respiration Jump-Starts Microbial Response to a Deep Oil Spill

David L. Valentine,[1]* John D. Kessler,[2] Molly C. Redmond,[1] Stephanie D. Mendes,[1] Monica B. Heintz,[1] Christopher Farwell,[1] Lei Hu,[2] Franklin S. Kinnaman,[1] Shari Yvon-Lewis,[2] Mengran Du,[2] Eric W. Chan,[2] Fenix Garcia Tigreros,[2] Christie J. Villanueva[1]

The Deepwater Horizon event resulted in suspension of oil in the Gulf of Mexico water column because the leakage occurred at great depth. The distribution and fate of other abundant hydrocarbon constituents, such as natural gases, are also important in determining the impact of the leakage but are not yet well understood. From 11 to 21 June 2010, we investigated dissolved hydrocarbon gases at depth using chemical and isotopic surveys and on-site biodegradation studies. Propane and ethane were the primary drivers of microbial respiration, accounting for up to 70% of the observed oxygen depletion in fresh plumes. Propane and ethane trapped in the deep water may therefore promote rapid hydrocarbon respiration by low-diversity bacterial blooms, priming bacterial populations for degradation of other hydrocarbons in the aging plume.

The oil leakage following the sinking of the Deepwater Horizon in the Gulf of Mexico was unprecedented because it occurred at 1.5-km water depth. The slow buoyant migration of petroleum from this depth allows time for dissolution of volatile hydrocarbons (*1*–*3*), including the natural gases methane (CH_4), ethane (C_2H_6), propane (C_3H_8), and butane (C_4H_{10}), that would readily escape to the atmosphere if released in shallow water. The resulting plumes of dissolved gas may co-occur with oil in the water (*3*) or may occur without oil because of gas fractionation processes during ascent (*4*). Based on the cumulative discharge estimates through 1 August 2010 (*5*) and a gas-to-oil ratio of 3000 ft^3 $barrel^{-1}$ (at atmospheric pressure), 1.5×10^{10} moles of natural gas were potentially emitted to the deep water over the course of the spill, in addition to the oil (*6*). We investigated the distribution, fate, and impacts of these hydrocarbons at 31 stations located 1 to 12.5 km from the active spill site (Fig. 1A) during the PLUMES (Persistent and Localized Underwater Methane Emission Study) expedition of the research vessel *Cape Hatteras*, 11 to 21 June 2010 (*6*).

In the vicinity of the leaking well, propane, ethane, and methane were most abundant at depths greater than 799 m and formed plume structures (Fig. 1C and figs. S1 to S3) with dissolved concentrations as high as 8 μM, 16 μM, and 180 μM for the three gases, respectively. These gases were orders of magnitude less concentrated at shallower depths, confirming suggestions (*7*), results from a noncalibrated spectrometric survey (*3*), and models (*1*, *2*) that the majority of the emanated gas dissolves or is otherwise partitioned (e.g., as gas hydrate) at depth and remains there. We defined a hydrocarbon plume by a methane concentration >500 nM, which is roughly 20 to 50 times as high as background levels of methane in the Gulf of Mexico (*8*) and is above the methane levels typically found around natural seeps (*9*–*13*). We observed deep (>799 m) hydrocarbon plumes at 29 of the 31 stations where methane measurements were made. One persistent plume at 1000- to 1200-m depth located to the southwest of the spill site (Fig. 1C) was identified previously (*3*, *14*–*16*). We also identified separate plumes at similar depths to the north and to the east, as well as a distinctive shallower plume at 800- to 1000-m depth also located to the east (figs. S2 and S3). The multiple plumes in opposing directions presumably originated at different times and indicate complex current patterns in the area before sampling.

The ratio of methane to ethane and propane varied substantially throughout the deep plumes. At the locations with highest hydrocarbon concentrations, the lower end-member values approached 10.85 for CH_4/C_2H_6 (Fig. 2A) and 19.8 for CH_4/C_3H_8 (Fig. 2B) and could therefore represent the gas ratios at the plume origin. Numerous locations display higher ratios, which we interpret as preferential loss of propane and ethane relative to methane, a pattern reported previously for biodegradation in hydrocarbon seeps (*17*). Variation in the C_2H_6/C_3H_8 ratio (Fig. 2C) further suggests preferential loss of propane compared with ethane, also an established biodegradation pattern (*17*). Methane's conservative behavior is supported by generally slow rates of oxidation, as measured with a tritium tracer approach (table S1).

Because bacterial propane, ethane, and methane consumption occurs with characteristic kinetic isotope effects (*17*), we measured the carbon isotopic composition of these gases in deep plume waters to assess the extent of their biodegradation. Samples with $CH_4/C_3H_8 > 19.8$ displayed a relative ^{13}C-enrichment in propane. Comparison of the ^{13}C-propane enrichment to the fractional loss of propane (Fig. 2D), determined from the CH_4/C_3H_8 ratio, indicates that biodegradation occurs (*18*, *19*) with an isotopic enrichment factor (ε) of –6.3. The value of ε for ethane (–11.8) based on CH_4/C_2H_6 ratios also suggests that biodegradation is occurring. Both values are similar to the minimum respective values of –5.9 and –11.2 determined from a previous mesocosm study (*17*). A lack of notable ^{13}C enrichment for methane [$\delta^{13}C\text{-}CH_4 = -61.1 \pm 2.2‰$ (per mil); $n = 18$] is further evidence of its conservative behavior in the fresh plumes.

To assess the importance of ethane and propane as aerobic respiratory substrates, we compared their loss patterns with observed oxygen anomalies in the deep-water column (Fig. 1B). Oxygen levels, measured in situ with an oxygen sensor and confirmed onboard ship through Winkler titrations, systematically declined in the plume horizon (Fig. 1D and fig. S4). Regression of the observed oxygen anomaly against the propane anomaly (*6*) indicates that 58% of the oxygen anomaly can be linked to propane (Fig. 3A).

[1]Department of Earth Science and Marine Science Institute, University of California, Santa Barbara, CA 93106, USA. [2]Department of Oceanography, Texas A&M University, College Station, TX 77843–3146, USA.

*To whom correspondence should be addressed. E-mail: valentine@geol.ucsb.edu